

Steady-State Characteristics of Spiral Groove Floating Ring Gas-Film Seal Considering Temperature-Viscosity Effect

W. Shipeng, D. Xuexing[†], D. Junhua and W. Jingmo

College of Petrochemical Engineering, Lanzhou University of Technology, Lanzhou, Gansu 730050, China

[†]Corresponding Author Email: dngxseal@126.com

(Received July 15, 2022; accepted November 27, 2022)

ABSTRACT

During the operation of the floating ring gas film seal, a certain amount of heat is generated inside the seal gap, giving rise to thermal deformation of the seal rings, and further leading to operation unstable and increased leakage rate. Based on the gas lubrication theory, the control equations of gas pressure and gas film thickness of the floating ring gas film seal are obtained. And the energy and temperature-viscosity equation are also introduced. The above equations were solved by the finite difference method and their correctness was verified by experiments. The variation of opening force, leakage rate, friction force, and gas film temperature rise with rotating speed, inlet pressure, and eccentricity were analyzed. The results reveal that, for leakage rate, the difference between the modeled and tested values is only 2.94% at high speeds, taking into account the influence of the temperature-viscosity effect. The experiment substantiates that the temperature-viscosity effect model is scientifically valid. Operation parameters also have different effects on sealing performance. Compared with isothermal flow, the pressure distribution in the gas film flow field will change significantly with increasing gas temperature, which means that the temperature-viscosity effect cannot be neglected in the flow field calculation. These results provide grounds for further study of the thermoelastic effect of air film seal of floating ring and have important engineering significance.

Keywords: Gas seal; Microgroove; Thermo-hydrodynamic lubrication; Hydrodynamic effect; Numerical simulation; Lubrication performance.

NOMENCLATURE

B	groove-dam ratio	P_i	inlet pressure
c_v	specific heat at constant volume	P_o	outlet pressure
C	gas properties	Q	leakage rate
e	eccentricity distance	r	shaft sleeve radius
f	friction force	T	gas temperature
F	opening force	T_i	inlet temperature
F_h	horizontal component of opening force	T_o	outlet temperature
F_v	vertical component of opening force	z	axial coordinate
h	medium film thickness	α	spiral angle
h_0	average film thickness	ΔT	temperature rise
h_g	groove depth	Δz	step width in axial direction
L	length of floating ring	$\Delta \theta$	step width in circumferential direction
n	rotational speed	ε	eccentricity ratio
n_z	number of grids in axial direction	η	gas viscosity
n_θ	number of grids in circumferential direction	η_0	medium gas viscosity value at temperature
N_g	groove number	θ	circumferential coordinate
O_j	center of the rotating shaft	ρ	gas density
O_r	center of the floating ring	ω	rotational angular speed of shaft
P	gas film pressure	Ω_1	non-groove region
		Ω_2	groove region

1. INTRODUCTION

The floating ring seal is an advanced non-contact seal. Its working principle is chiefly originated from gas lubricated bearing (Hou *et al.* 2020; Shi *et al.* 2020), and offers the advantages of no wear, low leakage, and compact structure. Therefore, it is widely applied to shaft seals of compressors, gas turbines, engines, and other equipment (Li *et al.* 2019). As rotating machinery develops towards high-parameters, extreme operating conditions exert a strong influence on the distribution of gas film pressure field and the change of gas temperature in the sealing device. In this context, thermal effect leads to the changes of parameters such as gas film clearance and gas viscosity, which have a decisive impact on the sealing performance and service life of the floating ring seal (Li *et al.* 2018; Andrés and Ashton 2010). Therefore, the temperature-viscosity effect is often an issue being considered in the design and performance prediction of floating ring seals.

Currently, in the academic literature, Ma *et al.* (2011a,b) demonstrated the influence law of thermal deformation caused by the rise of gas temperature which can form a divergent gap along the leakage direction on the sealing surface of the sealing device. Xie *et al.* (2020) elaborated the thermal deformation characteristics under high-temperature conditions, with a large temperature difference between the inner and outer diameter significantly diminishing the sealing performance. Zhang *et al.* (2019a,b) proposed the thermoelastic hydrodynamic lubrication model considering cavitation effect and temperature-viscosity effect by CFD method, and obtained that under high speed and heavy load conditions, the eccentricity was found to have a significant effect on oil film temperature. (Grigor'Ev and Fedorov 2019) integrated temperature-viscosity effects and cavitation phenomenon to solve for the pad surface temperature distribution of tilting pad bearings and experimentally verified the calculation results, which can be used as the basis for the design of tilting pad bearing. Luis and Tae (2010) proposed to couple the pressure governing equation with energy transfer equation with appropriate boundary conditions for the solution, and experimental data show that the gas film temperature at the middle plane of the gas foil bearing is higher than at the edge of the foil. Ding and Lu (2016) established a temperature field test system to compare the surface temperature of the gas film from theoretical calculations with the experimental test results, so that the theoretical model was verified to be correct and the temperature distribution in the dry gas seal was determined. Although a great deal of research has been completed by scholars around the world on thermoelastohydrodynamic problems, they have focused on carriers such as mechanical seals and air bearings. For floating ring seal, Xu *et al.* (2018) proved the dynamic characteristics of floating ring liquid film seal through a combination of CFD and test, in which the direct stiffness shifts from positive to negative as the seal length increases. Lu *et al.* (2020) considered the gas film eccentricity and

Rayleigh step problems, and proposed the central difference method to solve the multi-objective optimization function of cylindrical microgroove gas film seal, and observed that sealing pressure plays a key role in sealing operations. Ma *et al.* (2011a,b) used a particle swarm optimization algorithm to optimize the multi-dimensional groove geometry in the gas film seal and found that the influence of groove geometry size on the steady-state characteristics of the cylindrical gas film seal was not independent, and the optimal values of some seal device parameters were obtained. Xia *et al.* (2017, 2019) investigated the dynamic characteristics of the rotor of the floating ring seal, and found under high pressure conditions the seal structure would undergo elastic deformation, resulting in a degradation of the dynamic characteristics of the floating ring seal. Unfortunately, the above study of the floating ring sealing devices does not include a study of the influence of temperature-viscosity effect on sealing performance (Su *et al.* 2016; Guo *et al.* 2019). Alternatively, some calculation models simplify the real flow field changes in the seal gap while overlooking the change of temperature on the gas film viscosity, resulting in the deviations between theoretical calculations and experiment tests.

In this study, to accurately simulate the actual operation of the floating ring seal device. Based on the theory of gas thermodynamic lubrication, this paper takes the floating ring seal as the study objectives, and adopts the research method of combining numerical analysis and experiment on the premise of considering the temperature-viscosity effect. With opening force, leakage, friction, and gas film temperature rising as evaluation goals, the laws of rotational speed, pressure, and eccentricity on the performance of the floating ring seal considering temperature-viscosity effects are analyzed, and the research results offer a theoretical basis for the engineering design and application of the floating ring seal.

2. THEORETICAL MODEL

2.1 Geometrical Configuration

The floating ring seal belongs to dynamic pressure seals. Spiral micro-grooves are usually set on the outer surface of the shaft sleeve to increase the hydrodynamic effect (Joachimmiak and Krzyslak 2019, Joachimmiak 2020). When the shaft sleeve is rotated at high-speed, the medium gas will be carried into the spiral micro-grooves following the "pumping effect" on the high-pressure side. The medium gas will be continuously compressed at the root of the groove, creating a hydrodynamic effect in the micro-scale gap between the rotating ring and stationary ring. Moreover, the dynamic pressure effect of the micro-scale gap is further enhanced by using the eccentric installation between the sleeve and the floating ring to form a convergent wedge gap with different gas film thicknesses. The gas film stiffness can be increased to achieve a seal in the main leakage channel and improve the sealing performance of the floating ring sealing device. The

simplified geometric model of floating ring gas film seal system is shown in Fig. 1.

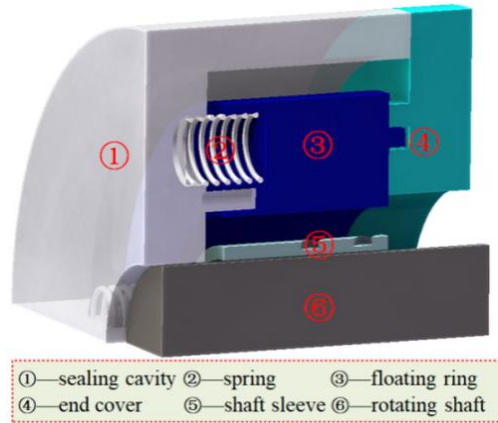


Fig. 1. Schematic diagram of floating ring sealing device.

2.2 Numerical Solution

2.2.1 Basic Assumptions

The flow field in the floating ring gas seal gap is a micro-scale flow field. To establish the flow control equations, the following assumptions are formulated for the lubrication model:

1. There is no relative slip of the medium gas at the interface of the seal pair.
2. The energy exchange due to heat conduction at the interface is neglected.
3. The viscosity and density of medium gas do not change in the direction of film thickness.
4. The medium gas flow belongs to the laminar flow.
5. The effect of centrifugal force and inertial force are ignored.

2.2.2 Pressure Governing Equation

According to gas lubrication theory, for the floating ring seal, the gas pressure distribution in the seal gap conforms to the Reynolds equation in cylindrical coordinates with the following results (Dyk *et al.* 2018) :

$$\frac{1}{r^2} \frac{\partial}{\partial \theta} \left(\frac{Ph^3}{\eta T} \frac{\partial P}{\partial \theta} \right) + \frac{\partial}{\partial z} \left(\frac{Ph^3}{\eta T} \frac{\partial P}{\partial z} \right) = 6\omega \frac{\partial}{\partial \theta} \left(\frac{Ph}{T} \right) \quad (1)$$

where r is the shaft sleeve radius, θ is the circumferential coordinate, P is the gas film pressure, h is the medium film thickness, η is the viscosity, T is the temperature, z is the axial coordinate, and ω is the rotational angular speed of the shaft.

2.2.3 Energy Governing Equation

The energy equation of compressible fluid in

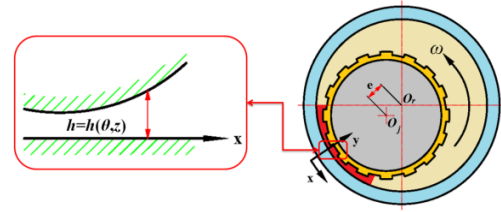


Fig. 2. Physical model of floating ring seal.

cylindrical coordinates can be written as (Bai *et al.* 2012) :

$$\left(\frac{h^3}{12\eta} \frac{\partial P}{r \partial \theta} - \frac{\omega r h}{2} \right) \frac{\partial T}{r \partial \theta} + \frac{h^3}{12\eta} \frac{\partial P}{\partial z} \frac{\partial T}{\partial z} = -\frac{\eta \omega^2 r^2}{h \rho c_v} + \frac{h^3}{12\eta \rho c_v} \left[\left(\frac{\partial P}{r \partial \theta} \right)^2 + \left(\frac{\partial P}{\partial z} \right)^2 \right] \quad (2)$$

where c_v is specific heat at constant volume.

2.2.4 Film Thickness Governing Equation

Figure 2 shows the model diagram of floating ring seal. In the diagram, O_j is the center of the rotating shaft, O_r is the center of the floating ring and e denotes the eccentricity.

The h is given by following equations:

$$h(\theta, z) = \begin{cases} h_0 & (\theta, z) \in \Omega_1 \\ h_0 + h_g & (\theta, z) \in \Omega_2 \end{cases} \quad (3)$$

where h_0 is average film thickness, h_g is groove depth, Ω_1 is non-groove region, and Ω_2 is groove region.

2.2.5 Temperature-viscosity Control Equation

When the inlet gas pressure is below 5MPa, the effect of gas pressure on viscosity is small, and only the viscosity of the gas as a function of temperature needs to be considered, which is solved for using the Sutherland equation (Ma *et al.* 1981):

$$\eta = \eta_0 \left(\frac{T}{T_0} \right)^{\frac{3}{2}} \frac{(T_0 + C)}{T + C} \quad (4)$$

where C is constantly correlated with gas properties, and 124k can be taken for air and η_0 is the corresponding medium gas viscosity value at temperature T_0 .

2.2.6 Computation Boundary Conditions

1. The pressure and temperature boundary conditions on the high and low-pressure sides of the sealing system using mandatory boundary conditions are as follows:

$$\begin{cases} z=0; P=P_i & z=1; P=P_o \\ z=0; T=T_i & z=1; T=T_o \end{cases} \quad (5)$$

where P_i is the boundary pressure at the high pressure side, P_0 is the atmospheric pressure, T_1 is the inlet temperature and T_0 is the outlet temperature.

2. Periodic boundary conditions for pressure and temperature with a period of 2π , as shown in the following equation:

$$\begin{cases} P(\theta, z) = P(\theta + 2\pi, z) \\ T(\theta, z) = T(\theta + 2\pi, z) \end{cases} \quad (6)$$

2.3 Seal Performance Parameters

The solution method adopted in this paper is the finite difference method (Zhang and Wang 2018; Wang *et al.* 2021). For the solution, the gas film in the sealing gap of the floating ring is expanded into a rectangle along the circumferential direction and divided into a discrete grid of $n_\theta \times n_z$. Among them, the density of mesh division is determined by calculation accuracy and calculation time. The air film field is meshed with a spacing of $\Delta\theta$ along the circumference and Δz along the axis. The convergence accuracy of the pressure field and temperature field is 10^{-6} . Fig. 3 demonstrates the meshing of the computation domain.

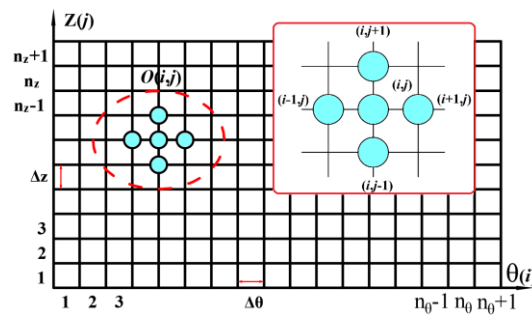


Fig. 3. Meshing of the computation domain.

The boundary conditions are brought into the grid to solve the governing equations, and the gas pressure field and gas film temperature field in the floating ring sealing system can then be obtained. The opening force, leakage, friction force, and gas film temperature rise of the sealing device are subsequently calculated to evaluate the sealing performance (Li *et al.* 2021). The flow chart for the numerical calculation of the floating ring seal is shown in Fig. 4.

1. The gas film opening force F can be expressed as follows:

$$\begin{cases} F_h = r \int_0^L \int_0^{2\pi} P \cos \theta d\theta dz \\ F_v = r \int_0^L \int_0^{2\pi} P \sin \theta d\theta dz \\ F = (F_h^2 + F_v^2)^{1/2} \end{cases} \quad (7)$$

where F_h and F_v denote the horizontal and vertical gas film opening force components, respectively, and F is total gas film opening force.

2. The gas leakage rate Q can be expressed as follows:

$$Q = r \int_0^{2\pi} \left(-\frac{h^3}{12\eta} \frac{\partial p}{\partial z} \right) \rho d\theta \quad (8)$$

3. The gas film friction force f can be expressed as follows:

$$f = \int_0^L \int_0^{2\pi} \left(-\frac{h}{2R} \frac{\partial p}{\partial \theta} + \frac{\mu\omega R}{h} \right) R d\theta dz \quad (9)$$

3. EXPERIMENTAL TEST

3.1 Experimental System

To verify the validity of the correctness of the calculation theory and the program codes in this

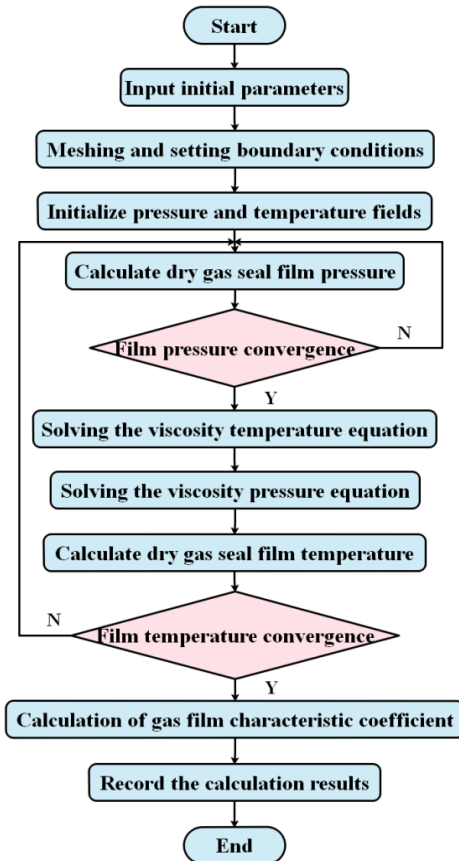


Fig. 4. Numerical calculation flow chart of floating ring seal.

paper, the sealing performance of the low pressure floating ring seal was tested experimentally. Parameters such as pressure, leakage, and gas film temperature of the medium gas in the seal cavity were measured, and the error between the theoretical results and experimental values was analyzed. During the test, the performance parameters of the floating ring seal were tested successively by adjusting the motor speed of the test-bed and the pressure of medium gas to provide the different working conditions demanded by the

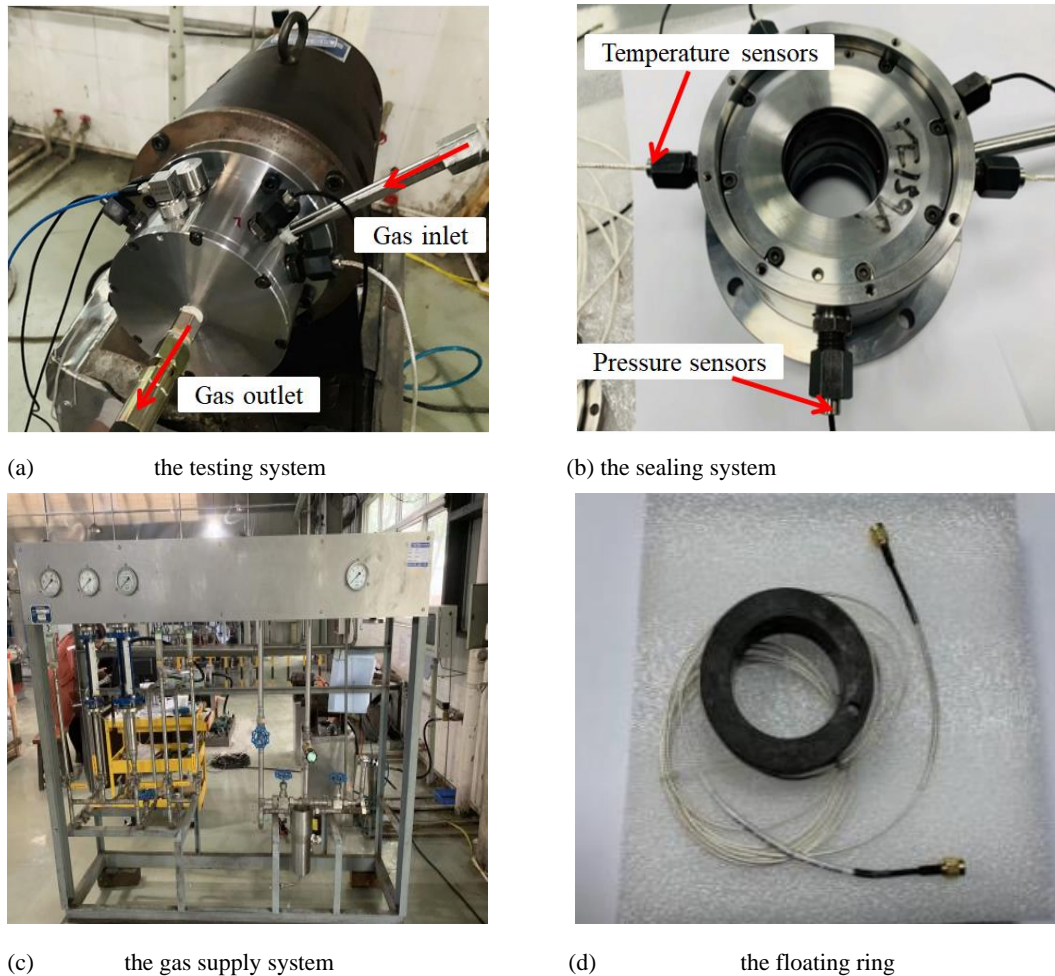


Fig. 5. Test loop of floating ring seal.

test. The floating ring seal experimental system mainly consists of a gas supply system, a transmission system, and a sealing system. The test devices are shown in Fig. 5.

3.1.1 Transmission System

Because the gap between the graphite sealing ring and the rotating shaft sleeve in the floating ring sealing device is only a few microns, and is mounted eccentrically, a high degree of precision and stability is required in the drive system of the test device. The bearing box must meet two requirements: small run out and the ability to withstand high speeds. The model parameters of the high-speed electric motorized are selected: the power of motorized spindle is 11KW, the voltage is 380V, the frequency is 50Hz, and the speed of high-speed motorized spindle can be freely adjusted within the range of 0-37000 r/min, as shown in Fig. 5 (a).

3.1.2 Sealing System

The floating ring sealing system adopts a back-to-back symmetrical structure to enable easy install and position. Particular attention is given to reducing friction between the surface of the floating

ring and the sealing end cover to ensure that the floating ring achieves a good opening force. The pressurized gas is supplied to the two sets of sealing devices simultaneously from the middle to ensure the dynamic balance of the sealing system, allowing for the stability of the air pressure, improving the stability of the test and ensuring the accuracy of test results, as can be seen in Fig. 5 (b).

3.1.3 Gas Supply System

The air supply system consists of metal float flowmeters, inlet pipes, and exhaust pipes. The pressure of medium gas is adjusted through a gas pressure regulating valve, which provides a pressure range of 0.1MPa to 3.5MPa. Due to the high requirement of gas film seal, the sealed medium gas needs to meet the requirements of drying and purity, so additional gas drying link is required during the design of the gas path system. The metal float flowmeters are adopted to observe the data of a gas of the sealing device, as shown in Fig. 5 (c).

3.2 Testing Principle

In this experiment, the rotating ring and stationary ring are made from silicon carbide and graphite, respectively. The gas gap distance between the

rotating ring and the stationary is on the order of microns, otherwise the test is difficult to respond to the sensor signal. The pressure sensors are installed inside the stationary ring by the landfill method to measure the gas pressure. The test data are collected by the LABVIEW program and converted into the opening force. For leakage, metal float flowmeters with high precision and precise response have been applied for leakage detection. This model LZZ-15 has an operating pressure of less than 0.9MPa, a float material of 316L, and a flow range of 0-4m³/h. In this paper, the volume flow obtained from the test is transformed into a mass flow. In this test, the landfill method was applied to arrange the pressure sensors, as shown in Fig. 5 (d). The pressure sensors were installed individually inside the through hole, and the floating torus should be kept flush with the end face of the probe during measurement. To ensure correct measurement, anti-interference measures were adopted during temperature measurement to minimize the interference so that the test requirements can be met.

4. VALIDATION

Based on the theory of thermohydrodynamic lubrication, the influence law of gas pressure distribution and gas temperature distribution in the sealing gap of the floating ring seal is explored. The parameters of the floating ring seal shown in Table 1 and Table 2 are adopted in the calculation process of this paper. The parameters are kept consistent except for the independent variables under study.

4.1 Theoretical Calculation

The installation of the floating ring seal devices is an eccentric installation. The circumferential film thickness is uneven. The axial distribution of spiral micro-grooves structure is not concentrated and symmetrical. Therefore, it is necessary to mesh and calculate the lubricating gas film of the overall sealing structure (Sun *et al.* 2021). As shown in Fig. 6, according to the structural characteristics of the floating ring seal, the gas film to be studied was extracted from it. The shape of the gas film thickness is similar to the cosine function, with the

thickness of the gas film in the non-grooved area being significantly higher than that in the groove area (Teixeira *et al.* 2017; Zhang *et al.* 2019c).

Table 1 Geometric parameters of the floating ring gas seal.

Parameters	Value
Outer radius of rotating ring, r (mm)	29.2
Groove-dam ratio, B	1:1
Groove depth, h_g (μm)	2
Groove number, N_g	16
Spiral angle, α ($^\circ$)	30
Length of spiral groove, L (mm)	30

Table 2 Working condition of the floating ring gas seal.

Parameters	Value
Average gas film thickness, h_o (μm)	5
Inlet pressure, P_i (MPa)	0.8
Outlet pressure, P_o (MPa)	0.101
Viscosity, η (Pa.s)	1.8×10^{-5}
Rotational speed, n (krpm)	16
Eccentricity, ϵ	0.7
Inlet temperature, T_i ($^\circ\text{C}$)	25
Density, ρ (kg/m^3)	1.1452

Based on the parameters in Tables 1 and 2, theoretical numerical calculations were carried out by using calculation codes. To observe the pressure drop and temperature change characteristics of the floating ring seal more visually, the cloud diagrams of the distribution of seal deceive gas film pressure field and temperature field at different rotating speeds (5000r/min, 10000r/min, 15000r/min and 20000r/min) and pressures (0.3MPa, 0.55MPa, 0.8MPa and 1.05MPa) as indicated in Fig. 7 and Fig. 8, respectively.

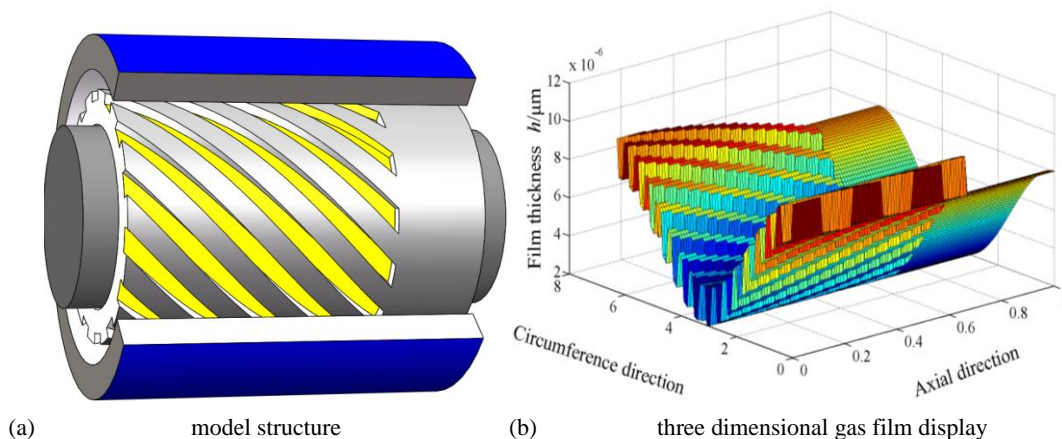
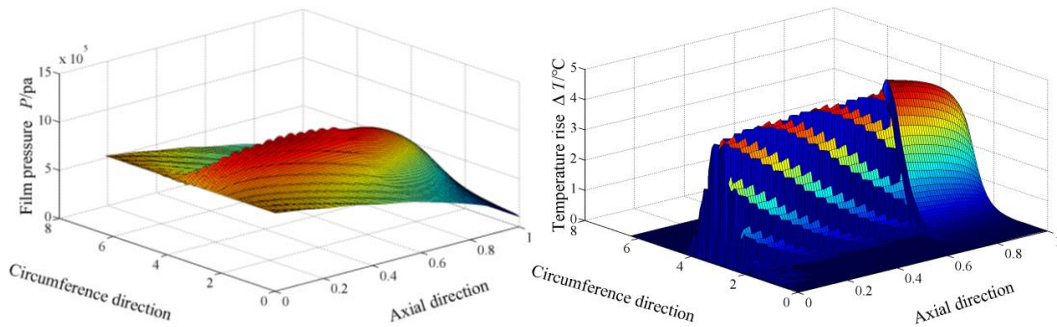
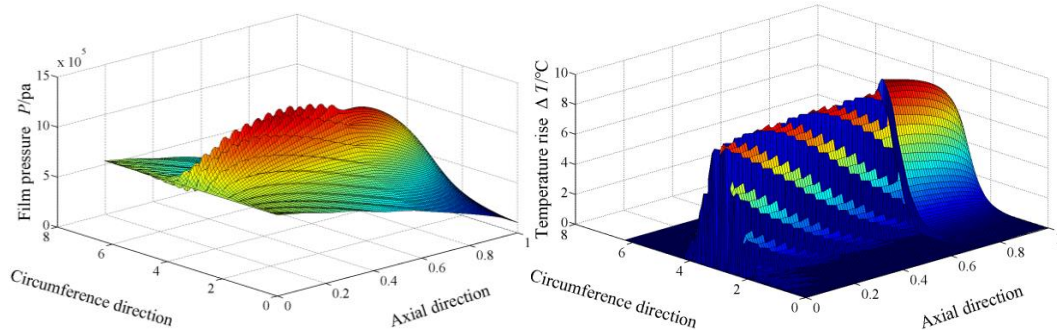


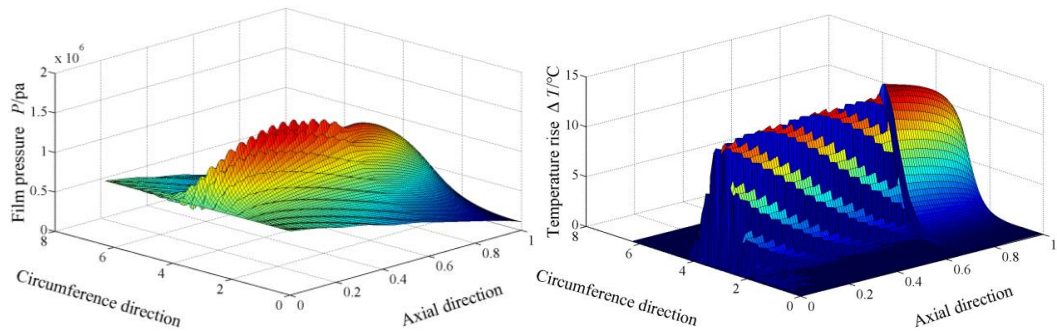
Fig. 6. Gas film thickness distribution of floating ring gas film seal.



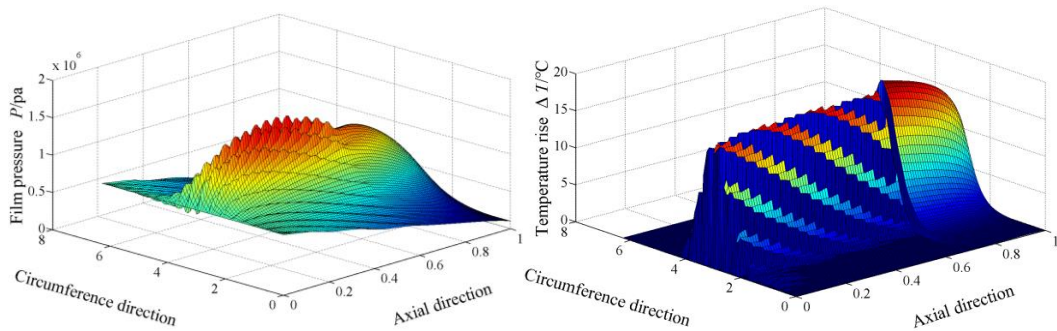
(a) $n=5000\text{r/min}$



(b) $n=10000\text{r/min}$



(c) $n=15000\text{r/min}$



(d) $n=20000\text{r/min}$

Fig. 7. Fields of gas pressure and temperature under different rotational speed.

As can be seen in Fig. 7, the pressure gradient of the floating ring seal shows an upward trend, with the gas temperature increasing significantly at the speeds of 5000r/min, 10000r/min, 15000r/min, and 20000r/min, respectively. From the gas inlet to the groove roots, the pumping effect of the spiral grooves leads to a cumulative extrusion of gas along the spiral grooves region, and the gas pressure has a maximum at the groove roots. The higher the rotating speed, the greater the maximal value of pressure. For the changing trend of gas temperature, a surprisingly different gas temperature distribution was found in the groove region, and it became more visible with the increase in rotating speed (Fuj and Yusa 2003; Zhong and Xie 2017). As mentioned above, by showing the three-dimensional diagram of gas film pressure and gas film temperature at different rotational speeds, it was found that the increase in rotational speed plays a dominant role in the increase of gas film temperature in the sealing gap.

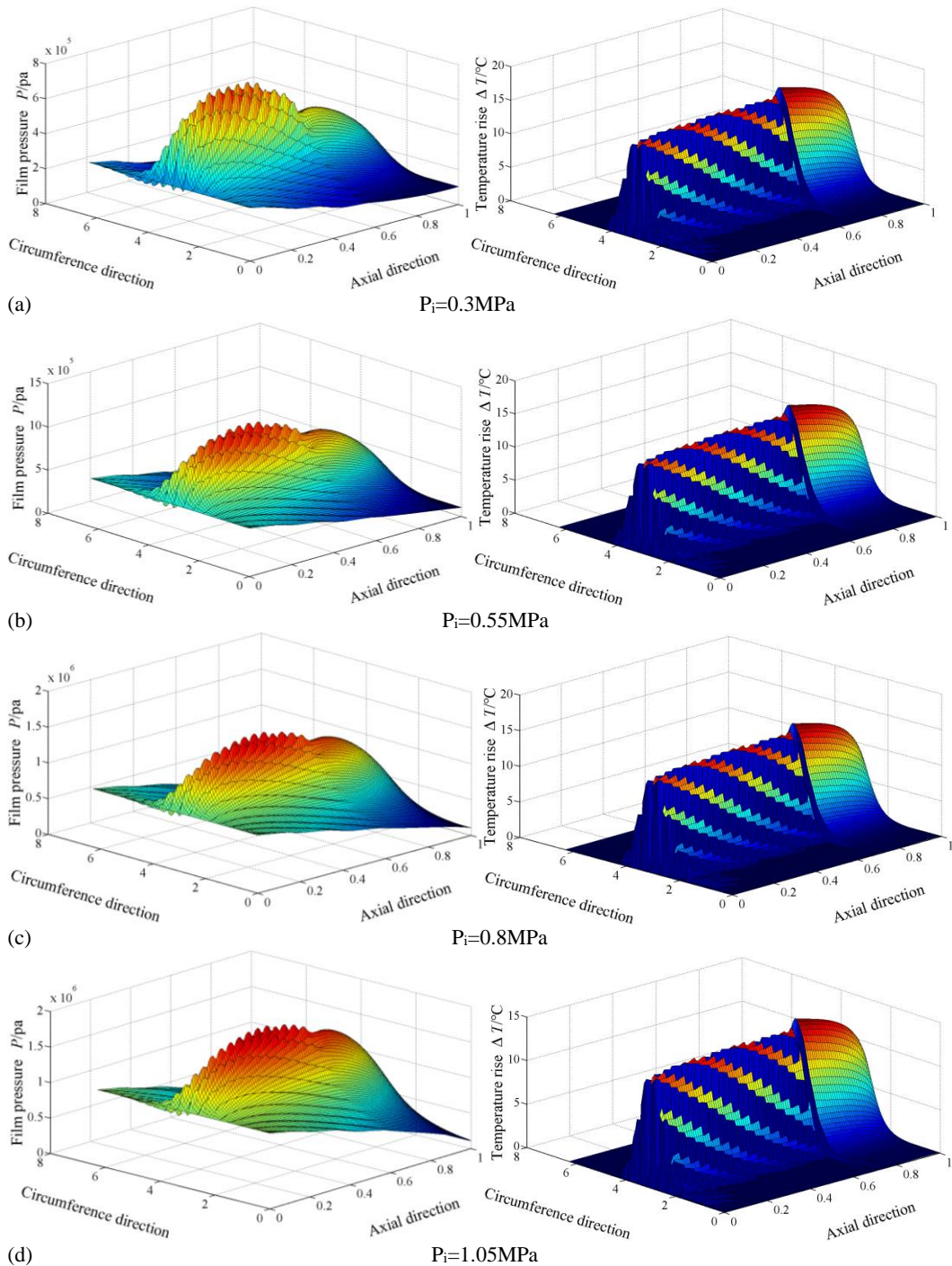


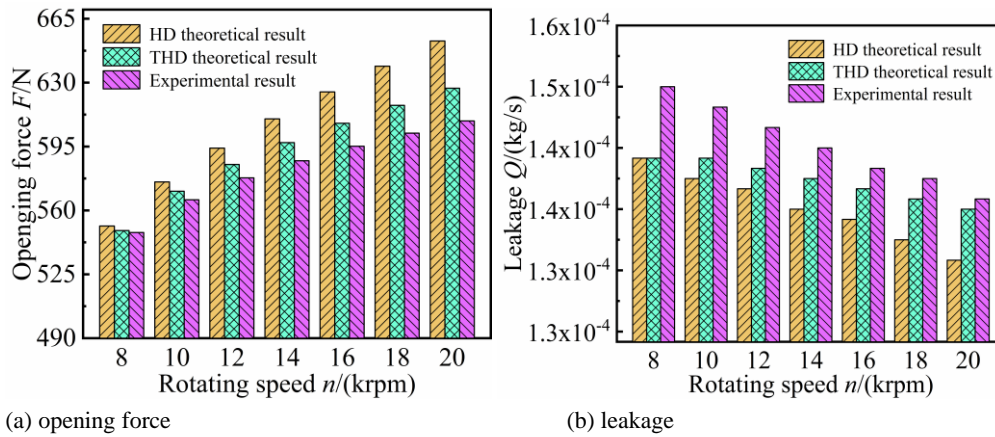
Fig. 8. Fields of gas pressure and temperature under different inlet pressure.

As can be seen in Fig. 8, the gas inlet pressure is 0.3MPa, 0.55MPa, 0.8MPa, and 1.05MPa, respectively. The maximum value of gas pressure increases with the inlet pressure, but the gas temperature of the floating ring seal gap gradually decreases. This phenomenon is mainly due to the change in pressure difference, which can increase the pressure of the whole gas gap region, making the value of gas pressure rapidly greater. When the pressure of the sealing medium is low, the gas expansion between the rotating pairs is weak (Shi *et al.* 2019, 2020), which gives rise to a decrease in the gas temperature. As the inlet pressure increases,

the flow rate of the medium gas and the velocity gradient also increases. The three-dimensional pictures of the gas film pressure and temperature at different pressures, as described above, reveal that the higher the gas film pressure, the stronger the gas film expansion in the sealing gap, and the more pronounced the drop in the gas film temperature at the outlet.

4.2 Test Verification

The gas film opening force and leakage volume of the floating ring seal device were obtained by



(a) opening force (b) leakage
Fig. 9. Distribution of the experimental and calculated values of the floating ring seal under different computational model.

setting up a test bench and selecting the working conditions of inlet pressure of 0.2MPa and rotating speed of 8000r/min to 20000r/min. The test values were compared with the theoretical calculation values to verify the accuracy and scientific validity of the theoretical model in this paper. As shown in Fig. 9, the HD model and THD model in the figure are the model considering hydrodynamic lubrication effect and the model considering the thermal hydrodynamic lubrication, respectively.

As shown in Fig. 9 (a), the gas opening force of the three models increases with the quick rotating speed. The opening force calculated by the theoretical models is significantly greater than the experimental value and the difference between them is quite striking as the speed of rotation increases. However, the change of gas temperature with viscosity was taken into account, making it more suitable to the variation law of the opening force measured in the test. Among them, at a speed of 20000r/min, the difference between the HD model value and test value is 7.18%, while the difference between the THD model and test value is only 2.94%.

Figure 9 (b) shows the leakage rate of the THD model is closer to the test value than that of the HD model. The leakage rate obtained from tests and theoretical calculations decreases with the increase of rotating speed, but the decrease is very small. At a rotating speed of 8000 r/min, the difference between the HD model and test value is 5.23%, and the difference between the THD model and test value is 4.76%. When the rotating speed is 20000r/min, the difference between the HD model and test value is 4.45%, and the difference between the THD model and test value is 1%. This indirectly confirms the validity of including THD in the calculation process.

Although the values of the experiment test and the theoretical calculation satisfy the error requirements, there are still some problems. The errors mainly arise from the following two aspects. For the test research, due to the particularity of the part structure, it is impossible to assemble more pressure sensors installed by the landfill method in a small area as well as the sensors. Due to the curved inner surface of the stationary ring, it is impossible to

accurately keep the probe of the pressure sensor perfectly flushed with the inner surface of the stationary ring, resulting in the sensor not being able to measure the gas pressure value correctly. For the theoretical calculations, installation errors and structure deformations are not factored in, which results in larger leakage rate and lower opening force than in the test. The opening force and leakage calculated by the THD model are relatively close to those of the experimental test values. However, there are still some deviations between the theoretical calculations of seal characteristics parameters and the test data, with maximum deviations of 3.26% and 5.19% for the gas film opening force and leakage rate, respectively. Therefore, accurate prediction of the sealing performance of the sealing device and the temperature distribution in the sealing gap is of prime importance for the long-life design requirements of dry gas seals.

5. RESULTS AND DISCUSSION

To further understand the steady-state characteristics of the floating ring seal system under the temperature-viscosity effect, the influence of different seal pressures, rotational speeds and eccentricities on the performance of floating ring seals is discussed in this section. In addition to the arguments to be discussed, the parameters in Table 1 and Table 2 are adopted in the calculations.

5.1 Rotational Speed

As shown in Fig. 10 (a), the gas film opening force increases linearly with the increase of the rotational speed. On the contrary, the opening force of the gas film decreases as the medium gas film thickness increases from $5\mu\text{m}$ to $8\mu\text{m}$. Because of the increase of rotating speed, the gas is squeezed into the micro-grooves by the pump effect, and the extrusion effect at the groove roots is also intensified, which gradually increases the opening force. However, with the increase of gas film thickness, the extrusion effect and regional high-pressure value decreases, leading to a decrease in the gas film

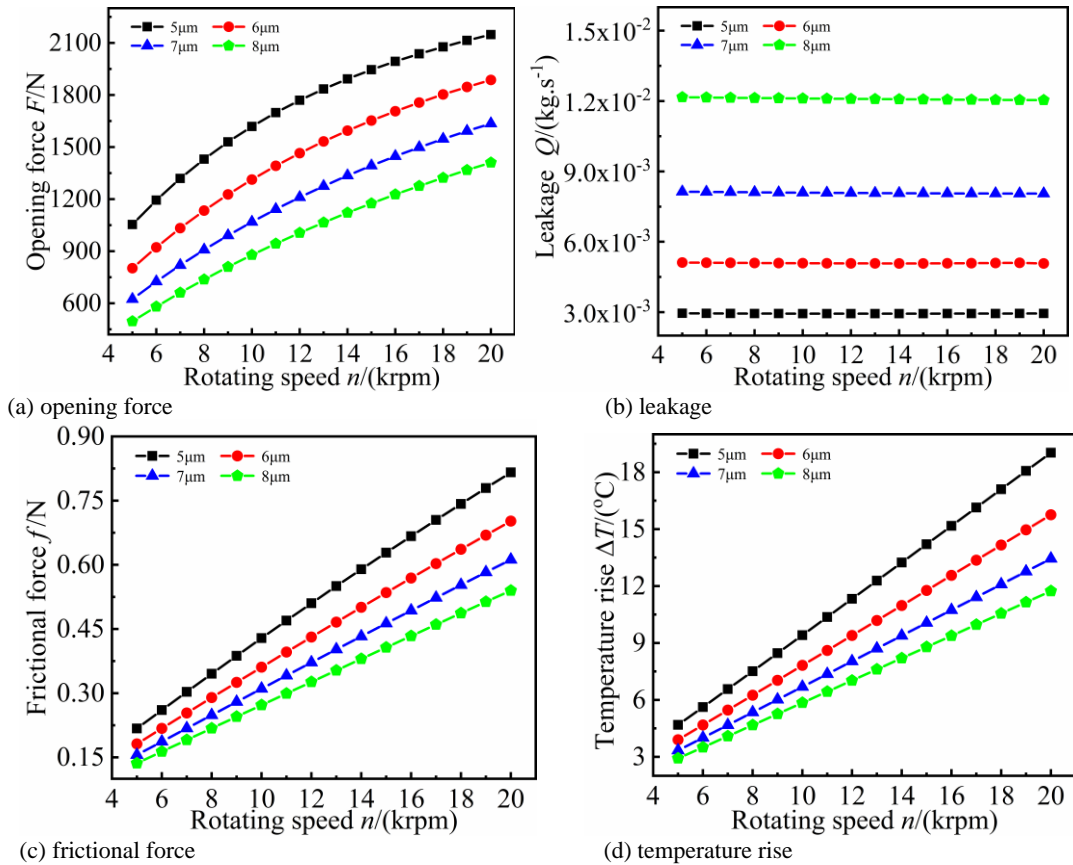


Fig. 10. Influence of rotational speed on sealing performance.

opening force of the floating ring seal. The difference between the maximum air film floating lift force and the minimum air film floating lift force is 737.61N.

Figure 10 (b) describes the influence of rotating speed on the leakage rate. By the increase of rotating speeding, the leakage rate decreases slowly by 2.85%. The larger the gas film thickness, the greater the leakage rate. Due to the narrow gap between the rotating ring and the stationary, the influence of rotating speed on the leakage rate is mainly induced by the effect of circumferential shearing speed on the flow field. With the improvement of rotating speed, the centrifugal inertia effect is also strengthened, which can raise the opening force of the gas film. When the pressure flow remains unchanged, the leakage rate decrease, but not significantly. As the gas film gap is narrow, the gas flows slowly, the gas film gap gets broadened, and the leakage rate also increases.

Figure 10 (c) illustrates the relationship between friction and rotating speed. It can be seen from the picture that the greater the rotating speed, the greater the friction of the gas film. When the rotating speed is small, the difference in friction difference for each film thicknesses is considerably close, while the difference increases as the rotational speed increases. It is attributed to the dynamic pressure effect of the gas in the micro-grooves on the surface of the shaft sleeve, which creates a thinner gas film. When the shaft sleeve is

rotating at high speed, there are Newtonian viscous shear force and viscous force between the gases, so that gas film friction is generated. The greater the speed, the larger the friction force. The viscosity of medium gas is generally low, results in overall low values of gas film friction. The maximum value is 0.82N.

As presented in Fig. 10 (d), the gas temperature rises with increasing of rotating speed. The larger the film thickness, the lower the gas temperature rises. The highest gas temperature is 19.02 C at a rotational speed of 20000r/min. This phenomenon is mainly due to the increase in gas viscous shear in the gap with the rise of rotating speed. The greater the friction force, the higher the gas temperature. The wider the gas film gap, the greater the leakage, and the heat leaks out with the leaking gas.

Therefore, a higher gas film thickness results in a smaller gas temperature rise.

5.2 Sealing Pressure

Figure 11 shows the effect of changing gas film pressure and film thickness on the sealing performance parameters of the floating ring seal. As can be found in Fig. 11 (a), the rise in gas pressure can greatly increase the opening force. The larger the gas film thickness, the lower the local high pressure. An increase in lift force of 1328.55N is observed as the gas film pressure increases when the air film thickness is as thin as 5 μm . When the

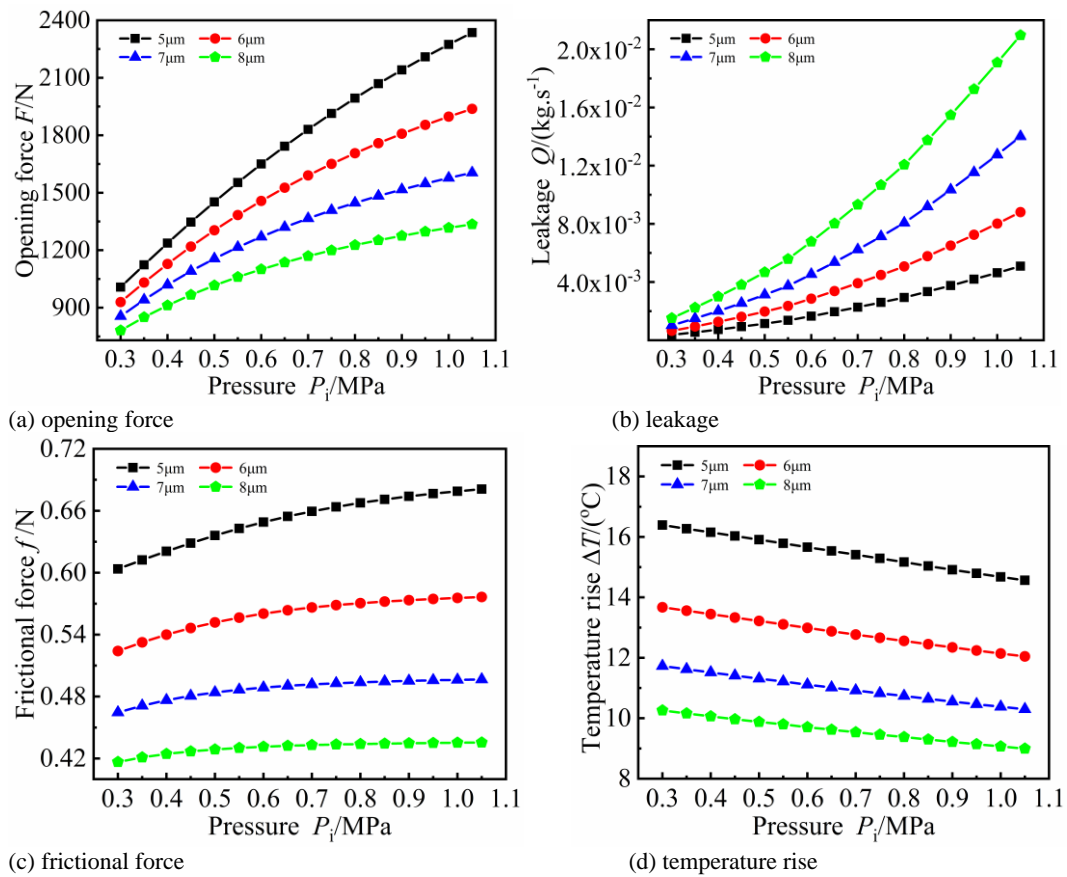


Fig. 11. Influence of sealing pressure on sealing performance.

film thickness is 8 μm , the lifting force of the film increases by 553.83N. It can be concluded from the observation of the variation pattern of the opening force that if the micro-grooves are placed on the high-pressure side, the rotating speed can only locally increase the gas film pressure. The change in pressure difference can increase the gas pressure in the whole gas film region, resulting in a rapid increase in the gas film opening force.

Figure 11 (b) expresses the influence curves of gas pressure on the leakage rate. The leakage rate rises approximately linearly with increasing inlet pressure; the leakage increases with the rise of gas film thickness. A corresponding increase in the gas film leakage rate is accounted for by the fact that when the velocity is held constant, the corresponding outlet density increases as the inlet gas pressure increases, causing an increase in the leakage rate.

Figure 11 (c) describes the relationship between the gas friction as well as the pressure and thickness of the gas film. The gas friction increases with pressure, and the trend of increasing friction tends to level off gradually. When the film thickness is at its thinnest, the friction of the film increases by 12.8% with increasing film pressure. An increase in film thickness leads to a decrease in friction. Because of the lower gas viscosity, the larger the pressure difference and the smaller the shear force, which makes the value of gas film friction smaller.

Figure 11 (d) illustrates the relationship between pressure, gas film thickness, and temperature rise in the wedge gap. The gas film temperature decreases with the increase of sealing pressure. Increasing the film thickness can lower the gas temperature. With the increasing sealing pressure difference, the gas leakage increases between the shaft sleeve and stationary ring, accompanied by heat transfer out with the leakage, so that the gas temperature between sealing surfaces decreases.

5.3 Eccentricity Ratio

Figure 12 demonstrates the influence of eccentricity on sealing performance. As shown in Fig. 12 (a), the eccentricity increases from 0.1 to 0.85, the gas opening force increases significantly. When the eccentricity is small, the influence of gas film thickness on the opening force is minimal. It is attributed primarily to the fact that when the eccentricity is small, the pumping effect of the grooves cannot be brought into play, causing the change of film thickness having little impact on the gas opening force. But as the eccentricity increases, the minimum gas film thickness is squeezed thinner and thinner, as a result, the wedge effect is enhanced. In the thicker parts of the gas film, the dynamic pressure effect of the grooves is greatly strengthened, so that the gas opening force becomes more available. This indicates that eccentricity is

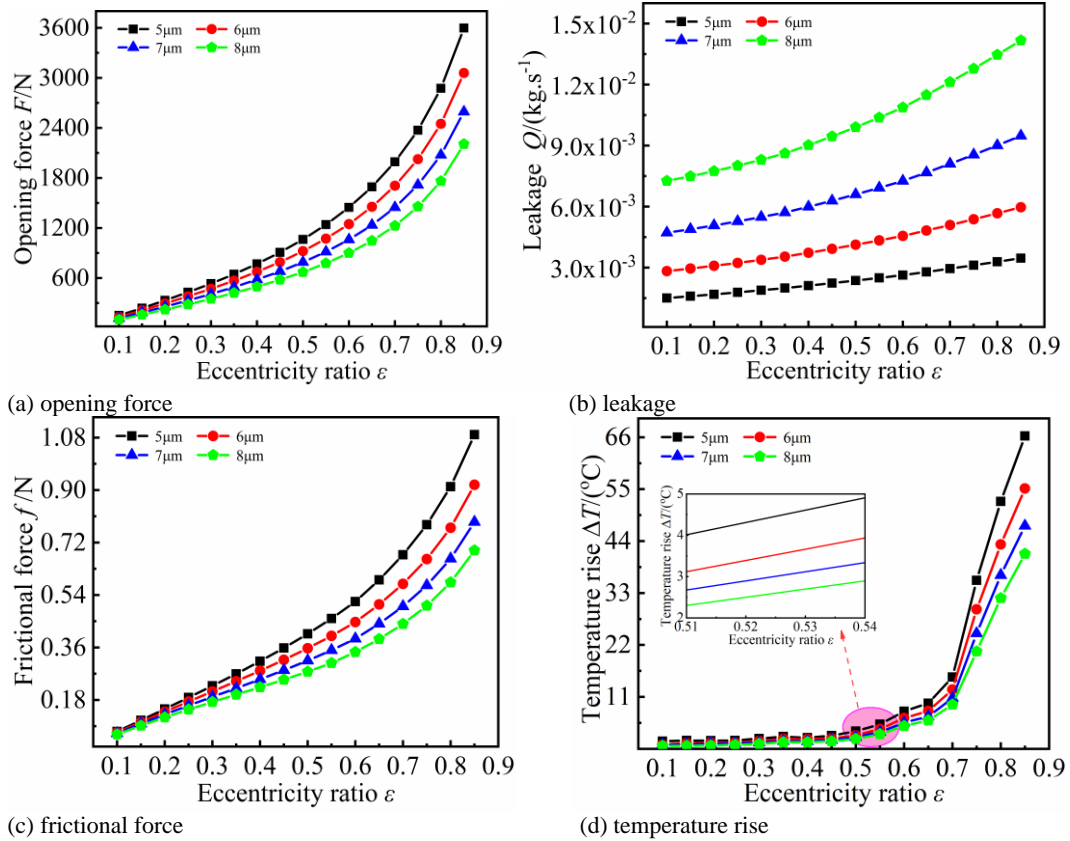


Fig. 12. Influence of eccentricity ratio on sealing performance.

the crucial parameter regulating whether the groove exerts a dynamic pressure effect.

Figure 12 (b) describes the influence curves of eccentricity on the leakage rate. With the increase of eccentricity, the inhomogeneity of gas distribution is enhanced, and the leakage rate under four kinds of film thicknesses rises significantly. With the film thickness increasing from 5μm to 8μm, the leakage rate increases by a factor of 1.30, 1.11, 1.01 and 0.95, respectively. However, the gas film gap is still the main factor influencing the leakage. This is mainly due to the carving of micro-grooves on the high-pressure side, where the increase in eccentricity results in a large gradient in gas film pressure and the pressure flow dominates the seal. At the same time, the axial direction flow increases at the maximal gas film thickness, resulting in the rapid rise of the seal leakage rate.

Figure 12 (c) depicts the relationship between gas friction and eccentricity. The influence of eccentricity on gas friction is similar to that of the opening force. An increase in eccentricity leads to an upward trend in gas friction. The maximum film friction force can reach 1.09N. The wider the film thickness is, the lower the gas friction is. However, a comparison of the effects of rotating speed and gas pressure on gas friction reveals that eccentricity has a greater effect on gas friction.

Figure 12 (d) expresses the relationship between gas friction and eccentricity. When the eccentricity is low, the gas film thickness has little effect on the gas temperature. When the eccentricity exceeds 0.7,

the gas temperature rises significantly. This is primarily because the eccentricity leads to a reduction in the thickness of the thinnest gas film thickness, an increase in the viscous shear effect of the gas in the air gap, an increase of gas temperature gradient and an increase in the gas temperature in the wedge gap due to heat conduction.

6. CONCLUSION

In this paper, a mathematical model of the floating ring seal system considering the temperature-viscosity effect are created by combining numerical calculation and experimental verification. The influence of rotating speed, pressure, and eccentricity on floating ring seals is discussed. The following conclusions can be drawn:

- The trend of test results is consistent with the theoretical results, indicating that the theoretical model is scientifically valid. The temperature-viscosity effect causes a significant change in the pressure and temperature distribution in the film flow field, which cannot be ignored in the flow field calculations.
- Increases in rotating speed, pressure, and eccentricity all increase the opening force of the gas film. Leakage increases significantly with the larger pressure and eccentricity, while decreasing gradually with increasing rotating speed. The value of gas friction

increases with the height of rotating speed, inlet pressure, and eccentricity. The gas temperature rises as the speed and eccentricity increase. However, as the inlet pressure intensifies, the gap gas temperature decreases.

- The greater the gas film thickness, the more pronounced the leakage under the same operating conditions, the bigger the range of reduction in opening force and gas film friction, and the lower the gas temperature.

ACKNOWLEDGEMENTS

The authors are grateful to the National Natural Science Foundation of China for funding support to this work (Grant No. 51565029).

REFERENCES

- Andrés, L. and Z. Ashton (2010). Comparison of leakage performance in three types of gas annular seals operating at a high temperature (300°C). *Tribology Transactions* 53(3), 463-471.
- Bai, S., X. Peng and Y. Meng (2012). Modeling of gas thermal effect based on energy equipartition principle. *Tribology Transactions* 55(6), 752-761.
- Ding, X. and J. Lu (2016). Theoretical analysis and experiment on gas film temperature in a spiral groove dry gas seal under high speed and pressure. *International Journal of Heat and Mass Transfer* 96, 438-450.
- Fu, J. and K. Yusa (2003). Measurement of force acting on a moving part of a pneumatic linear bearing. *Review of Scientific Instruments* 74(6), 3137-3141.
- Grigor'Ev, B. and A. Fedorov (2019). Thermohydrodynamic model of the tilting-pad journal bearing. *Journal of Machinery Manufacture and Reliability* 48(3), 236-242.
- Guo, H., S. Yang and S. Zhang (2019). Influence of temperature-viscosity effect on ring-journal speed ratio and stability for a hydrodynamic floating ring bearing. *Industrial Lubrication & Tribology* 71(4), 540-547.
- Hou, G., H. Su and G. Chen (2020). Performance analysis of compliant cylindrical intershaft seal. *Science Progress* 103(3), 003685042094195.
- Joachimmiak, D. (2020). Universal method for determination of leakage in labyrinth seal. *Journal of Applied Fluid Mechanics* 13(3), 935-943.
- Joachimmiak, D. and P. Krzyslak (2019). Analysis of the gas flow in a labyrinth seal of variable pitch. *Journal of Applied Fluid Mechanics* 12(3), 921-930.
- Li, G., Q. Zhang and E. Huang (2019). Leakage performance of floating ring seal in cold/hot state for aero-engine. *Chinese Journal of Aeronautics* 3(004), 11-23.
- Li, P., F. Zeng and S. Xiao (2021). Effects of texture bottom profile on static and dynamic characteristics of journal bearings. *Shock and Vibration*.
- Li, Z., Z. Fang and J. Li (2018). Numerical investigation on the leakage and rotordynamic characteristics for three types of annular gas seals in wet gas conditions. *Turbomachinery Technical Conference and Exposition* 141(3), 032504-1.
- Lu, J. (2020). Theoretical optimization and experiment on lubrication of floating microgroove cylindrical seal. *Industrial Lubrication and Tribology* 72(10), 1217-1226.
- Luis S. and H. Tae (2010). Thermohydrodynamic analysis of bump type gas foil bearings: a model anchored to test data. *Journal of Engineering for Gas Turbines and Power: Transactions of the ASME* 4, 042504-1-042504-10.
- Ma, C., S. Bai and X. Peng (2016a). Thermohydrodynamic characteristics of spiral groove gas face seals. operating at low pressure. *Tribology International* 95, 44-54.
- Ma, C., S. Bai and X. Peng (2016b). Thermoelastohydrodynamic characteristics of T-grooves gas face seals. *International Journal of Heat and Mass Transfer* 102, 277-286.
- Ma, G., Li, X., and Shen, X. (2011a). Multi-dimensional optimization of groove parameters in gas film seal. *Advanced Materials Research* 199-200, 1303-1307.
- Ma, G., W. Zhao and X. Shen (2011b). Analysis of parameters and performance for spiral grooved cylindrical gas film seal. *Procedia Engineering* 23, 115-119.
- Ma, P., B. Jiang and J. Zhang (1981). Critical assessment of viscosity and its correlation with temperature for gaseous substances under normal pressure. *Journal of Chemical Industry and Engineering* 32 (3), 193-205. (in Chinese).
- Dyk, Š., J. Rendl, M. Byrtus and L. Smolík (2018). Dynamic coefficients and stability analysis of finite-length journal bearings considering approximate analytical solutions of the Reynolds equation. *Tribology International* 130, 229-244.
- Shi, J., H. Cao and X. Chen (2019). Effect of angular misalignment on the static characteristics of rotating externally pressurized air journal bearing. *Science China Technological Sciences* 62(9), 1520-1533.
- Shi, J., H. Cao and X. Chen (2020). Effect of angular misalignment on the dynamic characteristics of externally pressurized air journal bearing. *Proceedings of the Institution of Mechanical Engineers, Part J: Journal of Engineering Tribology* 234(2), 205-228.
- Su, H., R. Rahmani and H. Rahnejat (2016).

- Thermohydrodynamics of bidirectional groove dry gas seals with slip flow. *International Journal of Thermal Sciences* 110, 270-284.
- Sun, X., P. Song and X. Hu (2021). Cross-scale flow field analysis of sealing chamber and end face considering the CO₂ real gas effect. *Journal of Applied Fluid Mechanics* 14(4), 979-991.
- Teixeira, J., A. Georgakis and C. Tibos (2017). Investigation of effective groove types for a film riding seal. *Journal of Engineering for Gas Turbines and Power: Transactions of the ASME* 139(7), 072503-1.
- Wang, Z., J. Zhu and N. Zhao (2021). A low dissipation finite difference nested multi-resolution WENO scheme for Euler/Navier-Stokes equations. *Journal of Computational Physics* 429, 110006.
- Xia, P., H. Chen and Z. Liu (2019). Analysis of whirling motion for the dynamic system of floating ring seal and rotor. *ARCHIVE Proceedings of the Institution of Mechanical Engineers Part J Journal of Engineering Tribology* 233(8), 135065011982937.
- Xia, P., G. Zhang and J. Zhao (2017). Investigations on rotordynamic characteristics of a floating ring seal considering structural elasticity. *Turbomachinery Technical Conference & Exposition* 50923, V07AT34A021.
- Xie, J., C. Ma and S. Bai (2020). Thermo-distortion characteristics of spiral groove gas face seal at high temperature. *Numerical Heat Transfer Fundamentals* 77(3), 242-256.
- Xu, R., Y. Hu and J. Yin (2018). A transient CFD research on the dynamic characteristics of liquid annular seals. *Annals of Nuclear Energy* 120, 528-533.
- Zhang, J. and J. Wang (2018). Numerical analysis for Navier-Stokes equations with time fractional derivatives. *Applied Mathematics & Computation* 336, 481-489.
- Zhang, Y., G. Chen and L. Wang (2019a). Effect of thermal and elastic deformations on lubricating properties of the textured journal bearing. *Advances in Mechanical Engineering* 11(10): 168781401988379.
- Zhang, Y., G. Chen and L. Wang (2019b). Thermoelastohydrodynamic analysis of misaligned bearings with texture on journal surface under high-speed and heavy-load conditions, *Chinese Journal of Aeronautics* S1000936118302681.
- Zhang, Y., S. Yu and C. Lu (2019c). An improved lumped parameter method for calculating static characteristics of multi-recess hydrostatic journal bearings. *ARCHIVE Proceedings of the Institution of Mechanical Engineers Part J Journal of Engineering Tribology* 234(2): 135065011985524.
- Zhong, L. and N. Xie (2017). The lubrication performance of water lubricated bearing with consideration of wall slip and inertial force. *Journal of Hydrodynamics Ser B* 29(1), 52-60.